

The characterization of the distant blazar GB6 J1239+0443 from flaring and low activity periods

L. Pacciani¹, I. Donnarumma¹, K. D. Denney², R. J. Assef³, Y. Ikejiri⁴,
M. Yamanaka⁴, M. Uemura⁵, A. Domingo⁶, P. Giommi⁷, A. Tarchi⁸,
F. Verrecchia⁷, F. Longo⁹, S. Rainó¹⁰, M. Giusti¹, S. Vercellone¹¹, A. W. Chen¹²,
E. Striani¹, V. Vittorini^{1,13}, M. Tavani^{1,13}, A. Bulgarelli¹⁴, A. Giuliani¹²,
G. Pucella¹⁵, A. Argan¹, G. Barbiellini⁹, P. Caraveo¹², P. W. Cattaneo¹⁶,
S. Colafrancesco^{17,18}, E. Costa¹, G. De Paris¹, E. Del Monte¹, G. Di Cocco¹⁹,
Y. Evangelista¹, A. Ferrari²⁰, M. Feroci¹, M. Fiorini¹², F. Fuschino¹⁹, M. Galli²¹,
F. Gianotti¹⁹, C. Labanti¹⁹, I. Lapshov¹, F. Lazzarotto¹, P. Lipari²², M. Marisaldi¹⁹,
S. Mereghetti¹², E. Morelli¹⁹, E. Moretti⁹, A. Morselli²³, A. Pellizzoni⁸,
F. Perotti¹², G. Piano^{1,13,23}, P. Picozza^{13,23}, M. Pilia^{24,8}, M. Prest²⁴,
M. Rapisarda¹⁵, A. Rappoldi¹⁶, A. Rubini¹, S. Sabatini¹, P. Soffitta¹,
M. Trifoglio¹⁹, A. Trois⁸, E. Vallazza⁹, D. Zanello²², C. Pittori⁷,

P. Santolamazza⁷, F. Lucarelli⁷, L. Salotti¹⁴ and G. Valentini¹⁴

¹*INAF/IAPS, Via Fosso del Cavaliere, 100 I-00133 Roma, Italy*

²*Marie Curie Fellow, Dark Cosmology Center, Niels Bohr Institute, University of Copenhagen, Copenhagen, Denmark*

³*NASA Postdoctoral Program fellow at the Jet Propulsion Laboratory, California Institute of Technology*

MS 169-236, 4800 Oak Grove Dr., Pasadena, 91109

⁴*Department of Physical Science, Hiroshima University, 1-3-1 Kagamiyama, Higashi-Hiroshima 739-8526, Japan*

⁵*Hiroshima Astrophysical Science Center, Hiroshima University, 1-3-1 Kagamiyama, Higashi-Hiroshima 739-8526, Japan*

⁶*Centro de Astrobiología (INTA-CSIC). PO Box 78, 28691 Villanueva de la Cañada, Madrid, Spain*

⁷*ASI Science Data Center, Via Galileo Galilei, I-00044 Frascati (Roma), Italy*

⁸*INAF-OAC, localita' Poggio dei Pini, strada 54, I-09012 Capoterra (CA), Italy*

⁹*Dip. Fisica, Univ Trieste and INFN Trieste, Via A. Valerio, 2, I-34127 Trieste, Italy*

¹⁰*Istituto Nazionale di Fisica Nucleare, Sezione di Bari, Via Orabona 4, I-70125, Bari, Italy*

¹¹*INAF-IASF Palermo, Via Ugo La Malfa 153, I-90146 Palermo, Italy*

¹²*INAF/IASF-Milano, Via E. Bassini, 15 I-20133 Milano, Italy*

¹³*Dip. di Fisica, Univ. Tor Vergata, Via della Ricerca Scientifica, 1 I-00133 Roma, Italy*

¹⁴*Agenzia Spaziale Italiana, Viale Liegi, 26 I-00198 Roma, Italy*

¹⁵*ENEA Frascati, Via Enrico Fermi, 13 I-00044 Frascati (Roma), Italy*

¹⁶*INFN-Pavia, Via Agostino Bassi, 6, I-27100 Pavia, Italy*

¹⁷*INAF-OAR, Via di Frascati, 33 I-00040, Monteporzio Catone (Roma), Italy*

¹⁸*School of Physics, University of the Witwatersrand, Johannesburg Wits 2050, South Africa.* ¹⁹*INAF/IASF-Bologna, Via Gobetti 101, I-40129*

²⁰*Dip. Fisica, Università di Torino, Via Giuria, 1, I-10125, Torino, Italy*

²¹*ENEA-Bologna, Via Martiri Montesole, 4 I-40129 Bologna, Italy*

²²*INFN-Roma La Sapienza, P.le A. Moro, 2 I-00185 Roma, Italy*

²³*INFN Roma Tor Vergata, Via della Ricerca Scientifica, 1 I-00133 Roma, Italy*

²⁴*Dip. di Fisica, Univ. Dell'Insubria, Via Valleggio 11, I-22100 Como, Italy*

ABSTRACT

In 2008 *AGILE* and *Fermi* detected gamma-ray flaring activity from the unidentified EGRET source 3EG J1236+0457, recently associated with a flat spectrum radio quasar (GB6 J1239+0443) at $z=1.762$. The optical counterpart of the gamma-ray source underwent a flux enhancement of a factor 15-30 in 6 years, and of ~ 10 in six months. We interpret this flare-up in terms of a transition from an accretion-disk dominated emission to a synchrotron-jet dominated one.

We analysed a Sloan Digital Sky Survey (SDSS) archival optical spectrum taken during a period of low radio and optical activity of the source. We estimated the mass of the central black hole using the width of the C IV emission line. In our work, we have also investigated SDSS archival optical photometric data and UV GALEX observations to estimate the thermal-disk emission contribution of GB6 J1239+0443.

Our analysis of the gamma-ray data taken during the flaring episodes indicates a flat gamma-ray spectrum, with an extension of up to 15 GeV, with no statistically-relevant sign of absorption from the broad line region, suggesting that the blazar-zone is located beyond the broad line region. This result is confirmed by the modeling of the broad-band spectral energy distribution (well constrained by the available multiwavelength data) of the flaring activity periods and by the accretion disk luminosity and black hole mass estimated by us using archival data.

Key words: galaxies: active - galaxies: quasars: general - galaxies: individual: GB6 J1239+0443 - radiation mechanism: non thermal

1 INTRODUCTION

Blazars are a sub-class of active galactic nuclei, emitting from radio to TeV energies. They are subdivided in two main categories: Flat Spectrum Radio Quasars (FSRQ) and BL Lacertae (BL Lac) objects. FSRQs are characterized by a flat radio spectrum in the GHz range (with spectral index $\alpha \leq 0.5$, where the flux density is $S_\nu \propto \nu^{-\alpha}$), and strong and broad emission lines (with equivalent width $> 5 \text{ \AA}$). BL Lac objects, on the other hand, have no or weak emission lines with equivalent width $< 5 \text{ \AA}$.

Blazars continuum emission originates from a relativistic jet aligned with the line of sight. Their Spectral Energy Distribution (SED) shows a double humped shape (Urry and Padovani 1995), with a low energy peak lying between IR and X-rays, and an high energy peak in the

MeV-TeV band.

The low energy region of blazar spectra is associated with the synchrotron emission coming from the jet relativistic electrons. The high energy region can be modeled through inverse Compton emission (leptonic models), with seed photons coming from an external region (e.g. the accretion disk, the dusty torus), eventually reprocessed by the broad line region, or the hot corona, or from the synchrotron process itself (synchrotron self-Compton, or SSC). A detailed description of leptonic models can be found in Maraschi et al. (1992); Marsher & Bloom (1992); Sikora et al. (1994).

The high energy region can also be modeled with hadronic scenarios (Mücke and Protheroe 2001; Mücke et al. 2003; Bottcher 2007), where the very high energy protons of the jet are radiatively important. The accelerated protons produce gamma ray emission through proton synchrotron emission, the decay of neutral pions, and synchrotron emission produced by secondaries.

The location of the so-called “blazar-zone”, i.e., the spatial location of the blazar SED-peaks and gamma-ray emitting region, in blazars is still a matter of debate. Sikora et al. (2008) proposed that the blazar-zone is located at 3–9 pc from the central engine for the outburst of 3C 454.3 (a bright FSRQ) occurred in 2005. For the same flare, Ghisellini et al. (2007) indicated, instead, a dissipation region at 0.5–0.8 pc from the central black hole (BH). From the combined study of time-dependent polarimetric radio images at 43 and 86 GHz, the optical polarimetry, and radio, optical, X-, gamma-ray light curves, Jorstad et al. (2010) proposed that the low and high energy emission is located near the 43 GHz core, at a distance of the order of tens of parsecs from the BH for 3C 454.3. A similar investigation, performed for the BL Lac objects OJ287 and AO 0235+164 (Agudo et al. 2011a,b), led to similar results.

Tavecchio & Mazin (2009) established that gamma-rays emitted inside the broad line region (BLR) are absorbed at $E > 20 \text{ GeV}/(1+z)$ due to the $\gamma\gamma$ interaction with the BLR photons (internal absorption). Poutanen & Stern (2010) refined this result, and claimed internal absorption features at $E > 5 \text{ GeV}/(1+z)$ and at $E > 20 \text{ GeV}/(1+z)$ in the gamma-ray spectrum of 3C 279, 3C 454.3, PKS 1510-08, and a few other FSRQ.

Within the leptonic scenario, Ghisellini & Tavecchio (2009) show that the contribution of external photon fields, including contributions from the BLR and dusty torus to the inverse Compton emission can be parametrized as a function of the accretion disk luminosity and the dissipation distance of the emitting blob from the BH (Ghisellini & Tavecchio 2009). Ghisellini et al. (2010) modeled the SED of the gamma-ray loudest blazars as being emit-

ted at 0.01–0.5 pc from the BH.

Using multiwavelength observations of the blazar GB6 J1239+0443, we will apply the models of Ghisellini & Tavecchio (2009) to further investigate the location of the blazar-zone. GB6 J1239+0443 was an unidentified gamma-ray source of the Virgo region (3EG J1236+0457), detected with low significance (Hartman et al. 1999; Casandjian & Grenier 2008) by the EGRET gamma-ray telescope (operating in the 30 MeV – 30 GeV energy range, see Esposito et al. 1999). In recent years the gamma-ray source has shown two episodes of remarkable high energy activity: at the beginning and at the end of 2008, when it was detected by the *AGILE* (Pacciani et al. 2009) and the *Fermi*–LAT (Tramacere et al. 2009) gamma-ray telescopes, respectively; then named AGL J1238+0406 (Pittori et al. 2009), and 2FGL J1239.5+0443 (Nolan et al. 2012). The accurate source location determined by *Fermi*–LAT allowed for the association of the unidentified gamma-ray source with BZQ 1239+0443 a flat spectrum radio quasar (FSRQ) included into the second edition of the Roma-BZCAT Multi-Frequency Catalog of Blazars (Massaro et al. 2010). The optical counterpart of this source is SDSS J123932.75+044305.3, located at $z=1.762$, and the radio counterpart is named GB6 J1239+0443. In the following sections, we refer to this object as GB6 J1239+0443, its radio source name.

Here we present the results of an analysis of multifrequency data simultaneous to the *AGILE* campaign on the Virgo field, and to the follow-up carried out after the *Fermi*–LAT detection and localization. By analysing the archival data, we estimate some fundamental physical properties of the source such as the accretion disk luminosity and the supermassive black hole (SMBH) mass. In this way we can obtain a consistent picture of the source emission in the framework of leptonic models of blazars for periods of both low and high emission activity. In Sections 2 and 3 we will describe the multi-wavelength campaigns related to this source. In Section 4 we will report on the archival data. In section 5 we will present our results consisting in the determination of the BH mass, the gamma-ray light curve and spectrum, and the SED modeling.

Table 1. Observing campaigns of the Virgo field during high gamma-ray activity periods from GB6 J1239+0443.

campaign	observatory	observing period
A	<i>AGILE</i>	from 2007 Dec. 16 17:14 to 2007 Dec 23 02:18 UT
		from 2007 Dec. 24 07:12 to 2007 Dec. 30 23:03 UT
		from 2008 Jan. 04 13:35 to 2008 Jan. 08 11:06 UT
	<i>INTEGRAL</i>	from 2007 Dec. 19 18:08 to 2007 Dec. 22 06:44 UT (revolution 633)
		from 2007 Dec. 25 17:39 to 2007 Dec. 28 06:27 UT (revolution 635)
B		from 2007 Dec. 31 17:13 to 2008 Jan. 03 04:00 UT (revolution 637)
	<i>Fermi</i>	Dec. 2008 – Jan. 2009
	Swift	from 2009 Jan. 02 17:47 to 2009 Jan. 04 20:21 UT* (total exposure 4.7ks)
	KANATA	2009 Jan. 02 18:14 UT for 1.5ks
		2009 Jan. 03 19:41 UT for 1.5ks

* Two pointings on 2009 Jan. 02 (exposure 2562 s and 380 s), and 5 pointings on 2009 Jan. 04 (exposure 597 s, 537s , 537 s, 577 s, 537 s)

2 GAMMA-RAY OBSERVATIONS AND RELATED MULTIFREQUENCY CAMPAIGNS

The *AGILE*–GRID gamma-ray telescope (operating in the 30 MeV – 50 GeV energy range, see Tavani et al. 2009) performed two observing campaigns of the Virgo field. The first campaign included 3 observations from 2007 December 16 to 2008 January 8. There were 3 simultaneous observations (revolutions 633, 635, 637) with the wide-field instruments aboard the *INTEGRAL* mission (operating in optical, hard X-, and soft gamma-rays, see Winkler et al. 2003). During this campaign *AGILE* detected high gamma-ray activity from GB6 J1239+0443 (Pacciani et al. 2009). In the following sections, we will refer to this time period as *period A*, and to the related multiwavelength campaign as *campaign A*.

AGILE also observed the Virgo field from 2009 June 4 to 2009 June 15, but there were no simultaneous observations with wide-field instruments operating at other wavelengths. GB6 J1239+0443 was undetected during this observation.

The *Fermi*–LAT gamma-ray telescope (20 MeV – 300 GeV, see Atwood et al. 2009), operating in all-sky survey mode since 2008 August 4, detected high gamma-ray activity at the end of December 2008 (Tramacere et al. 2009), and triggered optical-UV/X-ray observations with the Swift satellite (Gehrels et al. 2004), starting from 2009 January 2 for a total exposure of 4.7 ks. Optical V band photometry and polarization measurements were also made on-ground with the KANATA telescope on 2009 January 2 and on 2009 January 3 (Ikejiri et al. 2009). In the following sections, we will refer to the observations collected during this period as *period B*, and to the related multiwavelength campaign as *campaign B*. A summary of the observations is provided in Table 1.

3 DATA ANALYSIS

3.1 *AGILE*-GRID data

Level-1 *AGILE*-GRID data for campaign A were analysed using the *AGILE* Standard Analysis Pipeline (BUILD20) and the *AGILE* Scientific Analysis Package, based on the likelihood method (Mattox et al. 1996). Albedo photons were rejected by applying a cut at 85° centered on the Earth. We selected well-reconstructed gamma-rays by applying the FM3.119 filter, calibrated in the 100 MeV – 3 GeV energy band (Cattaneo et al. 2011). All the events collected during the passage in the South-Atlantic Anomaly were rejected. Counts, exposure and Galactic background gamma-ray maps were created with a bin-size of $0^\circ.1 \times 0^\circ.1$ for $E > 100$ MeV. We detected a source (AGL J1238+0406 in the *AGILE* catalog, see Pittori et al. 2009, and Verrecchia et al. 2011) with a significance of ~ 6 (as measured by the \sqrt{TS} parameter, see Mattox et al. 1996), located at $\alpha_{2000}=190.25$, $\delta_{2000}=4.40$, with an error radius of $(33 + 6)$ arcmin (statistical error at 95% confidence level -C.L.-, and systematic error, respectively), by integrating the GRID data for 4 days between 2008 January 4 13:35 and 2008 January 8 11:16 (within the campaign A). The source was positionally consistent with GB6 J1239+0443. A multisource maximum likelihood analysis was performed to extract the source flux and position taking into account nearby sources 3C 273, 3C 279, and 4C 04.42 (for which we obtained $\sqrt{TS} > 1$ from a preliminary analysis of the observing campaign). For AGL J1238+0406 we obtained a flux of $(62 \pm 9) \times 10^{-8}$ ph cm $^{-2}$ s $^{-1}$ ($E > 100$ MeV) and a photon index 1.92 ± 0.14 . The integration of the first week of observations with *AGILE* gave no detection at the position of GB6 J1239+0443, resulting in an upper limit of 21×10^{-8} ph cm $^{-2}$ s $^{-1}$.

3.2 *Fermi*-LAT data

We analysed the *Fermi* Large Area Telescope (*Fermi*-LAT) data for campaign B with the standard *Fermi* Science tools v9r23p1, following the prescriptions in the online documentation¹. We used the Pass 7 response functions (P7_V6). In particular, we selected events of *event class* 2, suitable for point-like sources, and we filtered out photons from the Earth's limb with a cut at 100° in the zenith angle. We performed the unbinned likelihood analysis inside a region of radius 15° around GB6 J1239+0443 to derive the source flux. We took

¹ <http://fermi.gsfc.nasa.gov/ssc/data/analysis/documentation/>

into account the diffuse backgrounds, which were modeled using `gal_2yearp7v6_v0` for the Galactic diffuse emission and `iso_p7v6source` for the extragalactic isotropic emission models², and all the 51 point-like gamma-ray sources in the second *Fermi*-LAT catalog (Nolan et al. 2012) within a slightly larger radius of 20° from GB6 J1239+0443 (we considered a larger radius due to the PSF width). For each source we used the model specified in the second *Fermi*-LAT catalog. For the sources within 10° from GB6 J1239+0443, we kept free all the spectral parameters in the fit. For the sources within an annulus of internal radius 10° and external radius 15° we kept free only the parameters related to the flux normalization, and all the other parameters were fixed to the values reported in the second *Fermi*-LAT catalog. For the sources outside 15° from GB6 J1239+0443, we fixed all the spectral parameters to the values reported in the catalog. This is a standard procedure for the analysis of *Fermi*-LAT data, implemented with the python routine *make2FGLxml.py*³ (contributed software by T. Johnson)

We proceeded with the analysis for energies only above 300 MeV, in order to process data with a smaller point spread function and reduce background gamma-rays from 3C 273, a bright and soft gamma-ray source ($\Gamma \sim 2.6$) located at $\sim 4^\circ$ from GB6 J1239+0443, since the 68% (95%) containment radius for *Fermi*-LAT at normal incidence is $4^\circ.5$ (10°) at 100 MeV⁴. Our study showed that this choice had a negligible effect on the signal significance of GB6 J1239+0443.

We used the *gtfindsrc* tool to locate the gamma-ray source. By integrating data for 1 month centered around the peak flux (2008 December 29 16:00 UT) in the band 300 MeV - 20 GeV, and by using photons converted both in the front- and back-section of the *Fermi*-LAT, we obtained a detection of a source (2FGL J1239.5+0443 in the second *Fermi*-LAT catalog, see Nolan et al. 2012) with $\sqrt{TS}=20$ located at $\alpha_{2000}=189.897$, $\delta_{2000}=4.718$ and an error radius of 9 arcmin. The source was positionally consistent with GB6 J1239+0443. We obtained a gamma-ray photon index of 2.15 ± 0.11 .

From the analysis in the 300 MeV – 20 GeV range, we also obtained a detection with $\sqrt{TS} \sim 18$, a flux of $(23 \pm 3) \times 10^{-8}$ ph cm⁻² s⁻¹, and a photon index of 2.21 ± 0.15 , when keeping the integration time within only 4 days centered at 2008 December 29 16:00 UT (the peak flux). During this integration period, the source was detected up to the energy

² both available on the URL <http://fermi.gsfc.nasa.gov/ssc/data/access/lat/BackgroundModels.html>

³ available on the URL <http://fermi.gsfc.nasa.gov/ssc/data/analysis/user/>

⁴ http://www.slac.stanford.edu/exp/glast/groups/canda/archive/lat_Performance.htm

interval 10–20 GeV, for which we obtained a detection with $\sqrt{TS} = 5.8$. To compute the upper limits needed to build the source light curve and spectra, we used the *UpperLimits* python function provided with the *Fermi* Science tools.

3.3 *INTEGRAL*/IBIS data

The *INTEGRAL*/IBIS (operating in the 17 – 400 keV energy range, see Ubertini et al. 2003) data for campaign A were processed using the OSA software version 8.0. We searched for the source starting from the images accumulated in the 20-40 keV band for revolutions 633, 635, 637 (simultaneous with *AGILE* observation of the Virgo field, campaign A). IBIS did not detect the source. We derived a 3 sigma upper limit of 1.7 mCrab for each revolution (200 ks exposure).

3.4 *Swift*-XRT data

The *Swift*-XRT (X-ray Telescope, operating in the 0.2 – 10 keV range, see Burrows et al. 2005) data for campaign B were processed using the most recent available calibration files. We made use of *Swift* Software version 3.5, FTOOLS version 6.8, and XSPEC version 12.5. The observations were obtained in photon counting mode, with a total integration of 4.7 ks. The mean source count rate was $(2.58 \pm 0.23) \times 10^{-2}$ cps. We extracted the spectrum using a photon binning ratio that ensured more than 20 photon counts per energy bin. We fitted the X-ray data with an absorbed power law, fixing the absorption to the galactic value of $1.85 \times 10^{20} \text{ cm}^{-2}$ (Dickey & Lockman 1990). We obtained a photon index of 1.42 ± 0.25 (90% C.L.). The estimated flux in the range 2-10 keV was $(8.8 \pm 2.7) \times 10^{-13} \text{ erg cm}^{-2} \text{ s}^{-1}$ (68% C.L.).

3.5 *Swift*-UVOT data

Swift-UVOT (Ultra-Violet/Optical Telescope, see Roming et al. 2005) data from each observation sequence of period B were processed by the standard UVOT tool `uvotsource` using the same version of the Swift software as for the XRT analysis. An extraction region of radius 5 arcsec centered on the source and a background region of radius 13 arcsec located at $\alpha_{2000} = 12^h 39^m 29^s.66$, $\delta_{2000} = +04^\circ 42' 34''.2$ (at least 27 arcsec far away from any object in the NED database) were used. Magnitudes are expressed in the UVOT photometric

system (Poole et al. 2008). We obtained $m_U=16.27\pm0.03$ for GB6 J1239+0443 (extinction corrected using the mean Galactic interstellar extinction curve from Fitzpatrick 1999).

3.6 Kanata optical data

The optical photometry was performed using TRISPEC (a simultaneous optical and near-infrared imager, spectrograph, and polarimeter, see Watanabe et al. 2005) attached to the Kanata 1.5-m telescope at Higashi-Hiroshima Observatory on 2009 January 2 at 18:14 and 2009 January 3 at 19:41 UT (period B). The observations were performed in *polarimetry-mode* with a narrow aperture mask of 1.5' width. The total exposure was 1476 s per night. The observations were pipeline-reduced, including bias removal and flat-field corrections. We derived the V-band magnitude from differential photometry with a nearby reference star at $\alpha_{2000}=12^h39^m30^s.11$, $\delta_{2000}=+04^\circ39'52''$. 6 of which the V magnitude of 14.095 was deduced from the g' and r' data in the 6th release of the Sloan Digital Sky Survey (SDSS, Adelman-McCharty et al. 2008).

3.7 *INTEGRAL*/OMC data

We analysed the OMC (Optical Monitoring Camera, equipped with a Johnson V filter, see Mas-Hesse et al. 2003) data collected during period A with the OSA software version 8.0. Due to the dithering mode of *INTEGRAL* observations, the field around the source was observed with OMC in the science windows 2, 50, 52, 78 of revolution 633, in the science windows 49, 51, 77 of revolution 635, and in the science windows 49 and 51 of revolution 637. To minimize readout noise contribution to the signal to noise ratio (S/NR), we selected snapshots of 200 s. Typically 6-10 snapshots of at least 200 s integration were recorded for each science window. Due to telemetry limits, the whole frame of the OMC field of view cannot be telemetred, but only sub-frames around sources from a reference catalog. GB6 J1239+0443 is included in one of the predefined sub-frames. We detected the source with $S/NR=4$ and $m_V=17.5\pm0.3$ with an aperture of 3×3 pixels, averaging the 3 revolutions. The investigation of previous *INTEGRAL* observations of the field resulted only in upper limits ($m_V > 18.1$ – 19.1 depending on the exposure of the observations). The Mosaic image from the individual snapshots taken during the multiwavelength campaign (obtained using the IRAF package) is shown in Fig. 1. The pixel size of the mosaic image was 1/3 of the OMC pixel to reduce spurious effects in the images shift. A cosmic ray signal was filtered

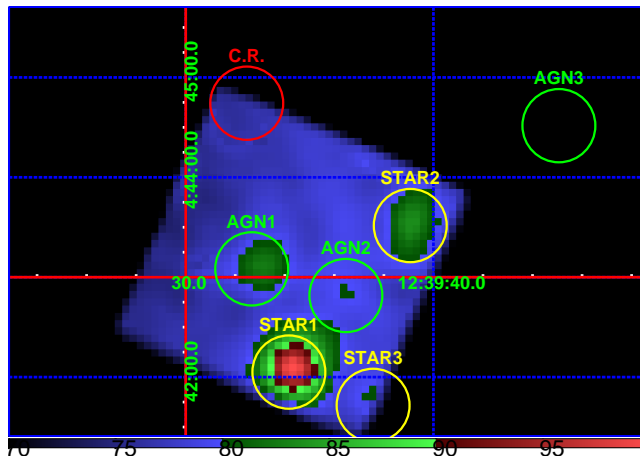


Figure 1. Mosaic image obtained with OMC simultaneous to the *AGILE* detection of gamma-ray flare of GB6 J1239+0443. The pixel size of the mosaic image is 1/3 of the original OMC pixel. The label *AGN1* is for GB6 J1239+0443 (SDSS J123932.75+044305.3), *AGN2* for SDSS J123936.52+044249.3, *AGN3* for SDSS J123945.06+044431.4. The circle marked *C.R.* indicates the filtered region where a cosmic-ray event was collected during revolution 635.

out (affecting the combined image around $\alpha_{2000}=12^{\text{h}}39^{\text{m}}32.5^{\text{s}}$, $\delta_{2000}=+04^{\circ}44'44.5''$), for science window 77 of revolution 635 only. This region is marked as C.R. in Fig. 1.

3.8 VLA archival data

We retrieved archival Very Large Array (VLA⁵) D-array 43 GHz data of GB6 J1239+0443, observed on 2001 November 5 for 65 s. The VLA data were reduced and analysed using standard routines implemented in the Astronomical Image Processing System (AIPS) package. The sources 3C 286 (1.45 Jy) and 1254+116 (0.43 Jy) were used as flux and phase calibrators, respectively.

An almost unresolved source has been detected at 43 GHz with position $\alpha_{\text{J2000}}=12^{\text{h}}39^{\text{m}}32.75\pm0.01^{\text{s}}$ and $\delta_{\text{J2000}}=04^{\circ}43'05.2\pm0.1''$, a peak flux density of $\sim 71.4\pm 3.6$ mJy, and an integrated flux density of $\sim 81.2\pm 4.1$ mJy.

4 THE ARCHIVAL DATA

In order to model accurately the SED (sections 5.2 and 5.4), we used archival data of GB6 J1239+0443 from the SDSS. Photometry with the filters u, g, r, i, z was performed on 2001 March 15. In particular the SDSS archive reports $m_u=20.62\pm 0.06$ and $m_g=20.47\pm 0.03$ (corresponding to $m_U \sim 19.9$, and $m_V \sim 20.5$). An optical spectrum (370–920 nm) was obtained on 2002 May 13.

⁵ The National Radio Astronomy Observatory is a facility of the National Science Foundation operated under cooperative agreement by Associated Universities, Inc.

Table 2. Summary of archival optical and radio observations of GB6 J1239+0443.

date	project/observatory	measurement description
2001 March 15	SDSS	optical photometry
2001 November 5	VLA	43 GHz
2002 May 11	Metsahovi	22 GHz
2002 May 13	SDSS	Optical Spectrum
2007 January 18	UKIDSS large Area Survey	near infrared photometry
2007 April 17 & May 13	GALEX	near UV photometry
2009 January 30	VLBA	15 GHz
2009 December 10	VLBA	15 GHz
2010 January 3–9	Planck	30 – 217 GHz

The near infrared photometry of the source was performed by using the data of the UKIDSS (UKIRT Infrared Deep Sky Survey) LAS (Large Area Survey) of 2007 January 18.

GALEX (an orbiting ultraviolet space telescope, see Martin et al. 2005) observed the source with NUV and FUV filters (with bandpass centered at 230 and 150 nm respectively) between 2007 April 17 and 2007 May 13.

The source was observed by VLA at 43 GHz on 2001 November 5, resulting in a low flux (we reported the analysis of this observation in the previous section).

A weak detection at 22 GHz was obtained by the Metsahovi observatory on 2002 May 11 (Terasranta et al. 2005), they reported a flux of 0.22 ± 0.04 Jy.

Following the *Fermi*–LAT detection of a gamma-ray flare, the source has been added to the MOJAVE⁶ sample, and was observed twice by VLBA in 2009 at 2 cm: on 2009 January 30 (one month after the gamma-ray flare) and on 2009 December 10. The source was found in the Planck legacy archive v0.5, with detections at 30, 100, 143, 217 GHz with observations on 2010 January 3, 2010 January 6, 2010 January 9, 2010 January 7, respectively. We also added the 147 GHz data for which the detection is flagged as *extended*. At last we included in the SED the detection in the *ROSAT* all Sky Survey. A summary of the archival observations is given in table 2, while the archival radio and optical SED is plotted in figure 2.

⁶ MOJAVE (Monitoring Of Jets in Active galactic nuclei with VLBA Experiments) is a long-term program to monitor radio brightness and polarization in jets of AGN.

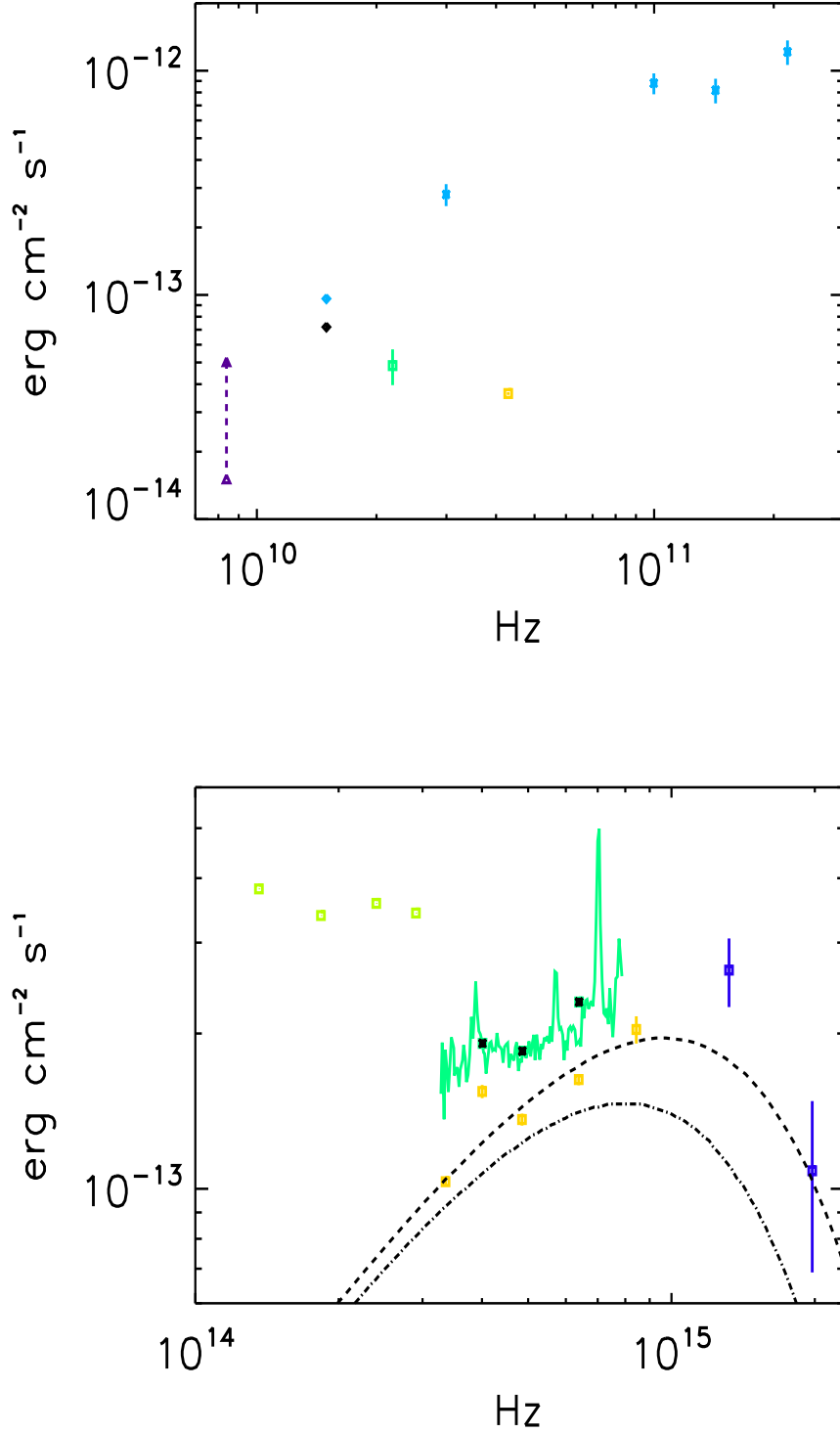


Figure 2. Top panel: archival radio observations of GB6 J1239+0443. Yellow box data was taken by VLA in 2001, Green data was taken by Metsahovi in 2002. Cyan diamond taken by VLBA in December 2009. Cyan stars are for Planck taken in 2010. Purple data represent the higher and lower fluxes measured at 8.4 GHz and reported in literature (from Mojave database). Bottom panel: archival optical observations of GB6 J1239+0443, all data are Galactic absorption corrected. Yellow squares are SDSS photometry taken in 2001; the green line is the SDSS optical spectrum taken in 2002 (squares of the same color with superposed black stars represent the simulated SDSS photometry evaluated from the observed spectrum). Light green squares show near-IR photometry taken by UKIDSS-LAS at the beginning of 2009, and blue squares are the GALEX data taken in mid-2007. The dashed and dot-dashed lines represent two disk-emission models; see text for details.

5 RESULTS

5.1 Disk luminosity and black hole mass determination from the archival optical/UV photometry

In spite of the large amount of data available for GB6 J1239+0443 the source has not been studied in detail before.

The optical SDSS spectrum was taken simultaneously with the 22 GHz Metsahovi radio observation (Terasranta et al. 2005). We note that the 22 GHz flux is a factor 3–4 lower than the Planck data of 2010 (light blue data in top panel of fig. 2). From the optical spectrum shape (bottom panel of fig. 2) and from the faint radio emission, a reasonable assumption is that the optical emission in May 2002 is accretion-disk-dominated. We evaluated the non-thermal dominance (NTD , see Shaw et al. 2012) of the optical spectrum making use of the C IV line luminosity, and the continuum luminosity extrapolated at 1350Å rest-frame.

We obtained $NTD=1.1^{+6.7}_{-1.0}$ where the major contribution to the errors comes from the uncertainties in equation (3) of Shaw et al. (2012), and $NTD=1.0^{+0.8}_{-0.5}$ making use of the Mg II line luminosity and the continuum luminosity at 3000 Å rest-frame, indicating that the optical spectrum taken in 2002 is typical of a thermal emission dominated source. We also observe that the optical photometry taken by SDSS in March 2001 results in a similar shape and lower flux ($\sim 30\%$ lower), and that the radio observation by VLA in November 2001 shows the source in a rather radio faint state. Therefore we also make the assumption of accretion disk dominated emission for the optical photometry taken in March 2001.

We compare the optical data taken by UKIDSS-LAS in January 2007, the SDSS spectrum taken in May 2002, and the optical photometry taken in March 2001. These observations taken at different epochs seem to demonstrate three different emission states: a jet-dominated emission state (UKIDSS-LAS), an accretion-disk-dominated state (SDSS photometry), and an intermediate state (SDSS optical spectrum) that seems to be dominated by accretion-disk emission with a possible minor contribution from the jet. We also note that the GALEX observations give a factor of ~ 10 lower flux with respect to the *Swift*/UVOT observation taken during the 2009 January flare. We cannot establish whether the UV emission detected by GALEX is due to the disk alone or whether there is also the contribution of the high energy tail of synchrotron emission. In the latter, unfavoured, case, the UV data from GALEX

result in at least an upper limit on the disk emission.

With these considerations, and assuming the disk emission is not variable on year timescales, we attempted to model the SDSS and GALEX photometry with a Shakura Sunyaev accretion disk (Shakura & Sunyaev 1973) around a non-rotating black hole (dashed curve in the bottom panel of Fig. 2). We modeled the disk emission as proposed by Ghisellini & Tavecchio (2009), with inner radius of 3 Schwarzschild radii (R_S), and outer radius of 500 R_S . We fit the model to the SDSS+GALEX data keeping free the parameters of disk luminosity (L_d) and R_S . We obtained a disk luminosity of $\sim 8.9 \times 10^{45}$ erg s $^{-1}$, and $R_S \sim 2.4 \times 10^{14}$ cm, corresponding to a maximum emitting temperature of $\sim 5.4 \times 10^4$ K, a BH mass of $\sim 8 \times 10^8$ solar masses, an accretion rate of $\sim 9 M_\odot y^{-1}$ (assuming an accretion efficiency $\epsilon_{accr}=0.1$), and then an Eddington ratio $R_{Edd} = L_d/L_{Edd} \sim 50\%$.

We note that one observation by SDSS and one observation by GALEX show a flux higher than the one expected according to our thermal emission model, but the filters used include quasar line emission from Mg II (the SDSS *i* filter) and Ly α (the GALEX NUV filter); see Figure 2. We also fit a disk model assuming the near-UV (GALEX) photometry is dominated by jet emission. In this case, the model assumes an accretion disk with only a minor contribution from jet emission and is fit to the SDSS data alone. In this scenario (dot-dashed curve in the bottom panel of Fig. 2), a model with a disk luminosity $> 5.4 \times 10^{45}$ erg s $^{-1}$ is required. We are aware that our model fits are not unique and that there are no simultaneous radio observations to strongly validate one fit over the other, but our preferred model reproduces the observed fluxes and is consistent with the scenario usually proposed for FSRQs (see for example Ghisellini et al. 2011, where hard optical/UV spectra are usually modeled as accretion disk dominated emission).

5.2 Black Hole Mass Determination from Archival Optical Spectrum

The BH mass of GB6 J1239+0443 could be estimated better by using the single-epoch BH mass scaling relationship for C IV derived from Vestergaard & Peterson (2006) and applied on the archival optical spectrum for this FSRQ. Unfortunately, the SDSS spectrum has a rather low S/NR (~ 3 per pixel in the continuum near the C IV $\lambda 1549$ emission line). Denney et al. (2009) show that line widths and thus single-epoch BH masses measured

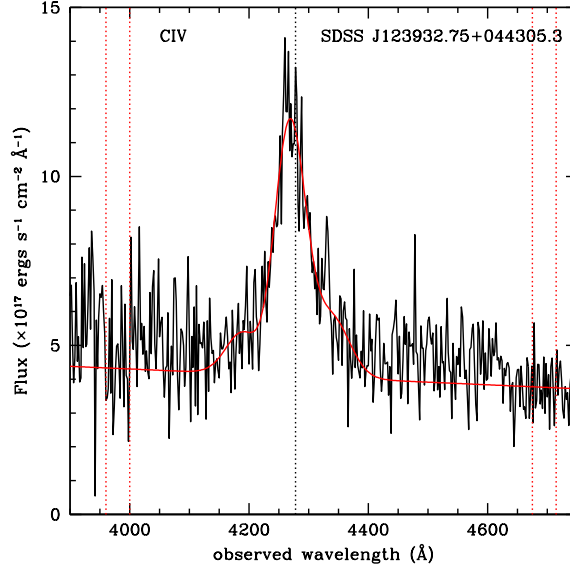


Figure 3. The C IV line in the archive optical spectrum of GB6 J1239+0443. The red continuum line is the fit with a sixth-order Gauss-Hermite polynomial.

from low S/NR data have relatively larger systematic uncertainties than those measured from high quality data. In addition, unrecognized absorption is a particular concern for low quality C IV data (see Vestergaard & Peterson 2006; Assef et al. 2011; Denney et al. 2011). Nonetheless, this is the only optical spectrum during a low state currently available. Therefore we use this spectrum to measure the line width and determine the mass. We employed two line width measurement methods and quote conservative uncertainties on the line width taking into account the low quality of the data. Our methods for measuring the C IV line width and uncertainties closely follow the prescription “A” described by Assef et al. (2011), and we therefore refer the reader to this work for details. After subtracting the linearly fit continuum, based on the windows shown in Fig. 3, we measured the FWHM of C IV both directly from the data ($\text{FWHM} = 2860 \pm 910 \text{ km s}^{-1}$) and from a sixth-order Gauss-Hermite polynomial fit to the line profile, as shown in Fig. 3 ($\text{FWHM} = 4710 \pm 390 \text{ km s}^{-1}$). Denney et al. (2009) show that direct measurement of the FWHM from low S/NR data systematically underestimates the line width, while measurement from a fit referring to the same data can overestimate the same width. We adopt a conservative approach and take the mean of these two width measurements and assume the quadrature sum of the uncertainties. The adopted FWHM measurement becomes $\text{FWHM}_{\text{CIV}} = 3800 \pm 1000 \text{ km s}^{-1}$. We then measure the mean continuum luminosity in the continuum window near rest-frame 1450 Å to be $\lambda L_{1450} = (3.47 \pm 0.44) \times 10^{45} \text{ erg s}^{-1}$, after correcting for Galactic extinction. We then evaluate the mass using equation (7) from Vestergaard & Peterson (2006), which

is also Equation (6) from Assef et al. (2011). It is worth noting that the SDSS spectrum does not extend to rest-frame 1350Å; however, Vestergaard & Peterson (2006) argue that the 1450Å luminosity can be substituted without penalty for the 1350Å luminosity, as we have done here. We estimate the BH mass of GB6 J1239+0443 to be $4.3_{-2.2}^{+3.2} \times 10^8 M_{\odot}$.

Assef et al. (2011) find a correlation between the ratio of the C IV-to-Balmer mass estimates and the UV-to-optical luminosity ratio. Since this correlation is based on the *ratio* of the mass estimates, barring further investigation into the source of this correlation, it is unclear whether it is the C IV-based or Balmer-based mass estimates, or both, to be the source of the bias. Regardless of origin, Assef et al. found that, when this correlation is removed, and when they arbitrarily choose to correct the C IV-based masses, the corrected masses are highly consistent with the measured Balmer-line-based mass estimates (the scatter in the corrected C IV vs. Balmer mass estimates is reduced by a factor $\gtrsim 2$ when compared to the uncorrected mass estimates; see Assef et al. 2011). Balmer-based mass estimates are generally more accepted in the literature because they are relatively better calibrated with direct mass measurements from reverberation mapping (see, e.g., Collin et al. 2006; Vestergaard & Peterson 2006; Denney et al. 2009). At this point, however, it is impossible to state which of the two mass measures is actually more accurate. In particular, we must consider that host galaxy starlight can significantly contaminate the optical luminosity with which Balmer-based masses are estimated, yet there may be evidence of non-virial motions from C IV (see, e.g., Richards et al. 2002). For GB6 J1239+0443, we fit a powerlaw continuum to the full wavelength extent of the SDSS spectrum and extrapolate to rest-frame 5100Å to estimate the rest-frame optical luminosity to be $\lambda L_{5100} = (2.64 \pm 0.33) \times 10^{45} \text{ erg s}^{-1}$. Using equation (8) of Assef et al. (2011), with the coefficients based on their prescription A, we can then calculate a corrected C IV-based BH mass of $5.3_{-3.3}^{+4.4} \times 10^8 M_{\odot}$.

The two mass estimates (based on the C IV broad line width and on the thermal continuum) are in qualitative agreement.

5.3 Gamma-ray light curve

We created a gamma-ray light curve for the source from both the *AGILE* pointing and the *Fermi* survey, as shown in Fig. 4. The *AGILE* data were integrated with bin sizes of about 6.5, 6.5, and 4 days, due to gaps in the observation (see Table 1). The *Fermi*-LAT data were integrated with binsizes of 1 and 7 days. The flux reported is in the 100 MeV - 3 GeV range

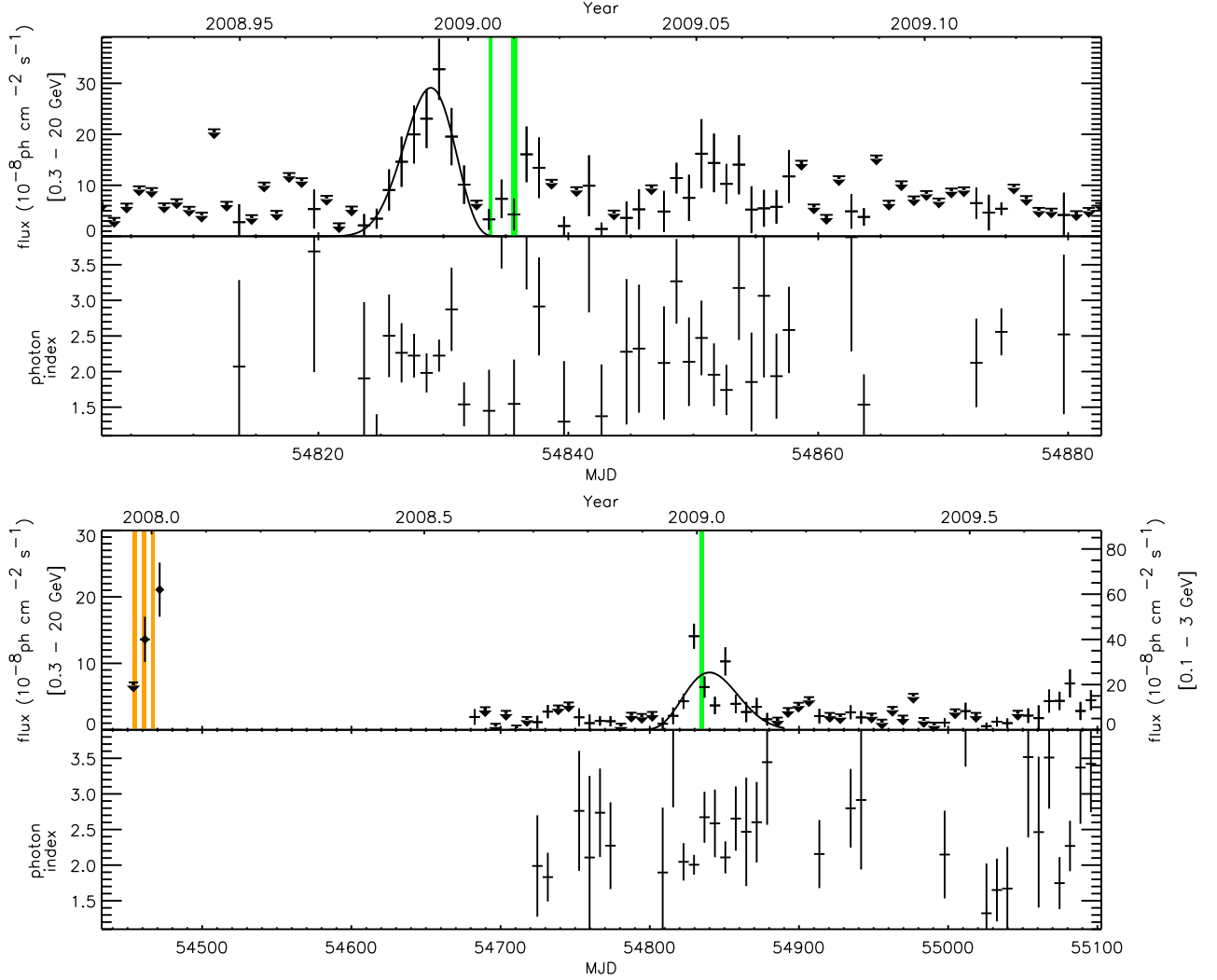


Figure 4. The gamma-ray light curve for GB6 J1239+0443 obtained with *AGILE* during campaign A (diamond symbols and right vertical scale for the gamma-ray flux) and *Fermi* (left vertical scale for the gamma-ray flux). For the *Fermi*-LAT data we report also the photon index evaluated in the 300 MeV - 20 GeV energy band. The upper panel reports *Fermi*-LAT data with a typical binsize of 1 day. The lower panel reports *Fermi*-LAT data with 7 days integration. *AGILE* data were integrated with bin sizes of about 6.5, 6.5, 4 days, due to gaps in the observation (see Table 1). The orange bands represent the *INTEGRAL* campaign (campaign A); width is in scale. The green bands represent the *Swift* campaign (campaign B); width not in scale.

for *AGILE*. As discussed in section 3, the *Fermi*-LAT data were analysed between 300 MeV and 20 GeV in order to reduce the contamination from the nearby 3C 273 at lower energies. In Fig. 4 we also report the gamma-ray photon index in the 300 MeV - 20 GeV as obtained by the *Fermi*-LAT data assuming a power-law spectrum.

To evaluate the flare duration, we made use of the procedure described by Abdo et al. (2010). From the light curve with time bin of 1 day, we obtained a duration (defined as $\frac{T_{rise} + T_{fall}}{2}$) of 7 days and an asymmetry -0.3 (see Abdo et al. 2010 for details, T_{rise} and T_{fall} are the rising and falling time respectively). The light-curve with time bin of 7 days shows more than a single relative maximum; therefore, the fit with a simple curve is not feasible. A

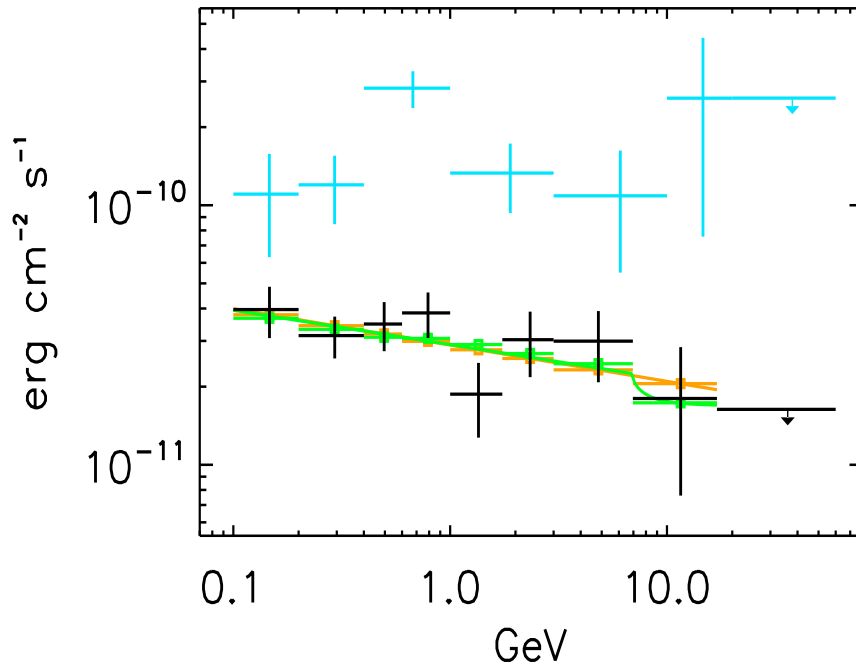


Figure 5. Gamma-ray spectrum of GB6 J1239+0443 integrated for one month around the peak flux (black data). The spectrum integrated for 4 days around the flare is reported too, multiplied by a factor 2 (cyan data). The fitted models discussed in the paper are reported. The continuous lines are for the models, the binned curve are for models weighted over each energy bin. The power law model is reported in orange, the power law model + gamma-gamma absorption is reported in green.

rough definition of the gamma-ray activity period could instead be the timespan for which *Fermi*-LAT detects gamma-ray emission from the source. Assuming temporal bins of 7, 15, and 30 days, we found that *Fermi*-LAT detected gamma-rays from the source for at least 11 weeks.

5.4 The *Fermi*-LAT gamma-ray spectrum for the high activity period of campaign B

The gamma-ray spectrum obtained by *Fermi*-LAT data, integrated for one month centered around the peak flux (2008 December 29 16:00 UT), is reported in Figure 5 together with the spectrum integrated for four days. The 30-day integrated spectrum has been fit first with a power-law model. Because absorption is expected for a blazar-zone originating near the central source (e.g., within the BLR), we also fit the spectrum with a power-law combined with absorption. In particular, absorption at $E > 20 \text{ GeV}/(1+z)$ is expected (Tavecchio & Mazin 2009) due to the Ly continuum, or at $E > 5 \text{ GeV}/(1+z)$ due to the He II recombination continuum (Poutanen & Stern 2010). We therefore fit the gamma-ray

Table 3. Gamma-ray spectral properties of GB6 J1239+0443, uncertainties at 68% C.L.

Power Law		Power Law + Double Absorber			
χ^2/DoF	photon index	χ^2/DoF	photon index	τ_H	τ_{He}
1.1	2.14 ± 0.08	1.6	2.13 ± 0.08	$1.0^{+4.6}_{-1.0}$	$0^{+0.9}_{-0}$

spectrum of GB6 J1239+0443 with a power-law combined with the gamma-gamma absorption model as proposed by Poutanen & Stern (2010). Here, the absorption was fit with two parameters: (1) the optical depth for the H I complex (τ_H) and (2) the optical depth for the He II complex (τ_{He}). We fit the models to the data for gamma-ray energies below 20 GeV, because the extragalactic background light is expected to absorb gamma-rays of $E \gtrsim 20$ GeV, for sources at the redshift of GB6 J1239+0443 (Finke et al. 2010). The results of the fit are reported in table 3. The fit with the gamma-gamma absorption components results in no absorption from the He II complex, and weak absorption from the H I complex. We performed the F-test on the two fits reported in table 3 to test the hypothesis of the need of the absorption components. The F-test gives a value of 0.15, and an associated probability of $\sim 87\%$, hence the absorption component is not necessary to fit the spectrum, suggesting that in GB6 J1239+0443 the blazar zone is located in the outer low-ionization region of the BLR or outside it.

5.5 The spectral energy distribution for the high activity periods

We constructed two spectral energy distributions referring to the high gamma-ray activity observed by *AGILE* and *Fermi* (campaigns A and B, respectively, as reported in Table 1) with the data collected so far. The *AGILE* data are integrated for 4 days (the duration of the last observation during the campaign A, from 2008 January 4 13:35 to 2008 January 8 11:06 UT). The *Fermi*-LAT data for period B are integrated within 4 days around the flux peak (2008 December 29 16:00 UT) to achieve acceptable statistics. These spectral energy distributions are shown in Figure 6, where we also included the archival data.

The SED modeling has been performed in the framework of leptonic models. We assume that the emitting region is a spherical blob of radius R_{blob} , with bulk Lorentz factor Γ_{bulk} , an electron population distribution proportional to $\frac{(\gamma/\gamma_b)^{-s_1}}{1+(\gamma/\gamma_b)^{-s_1+s_2}}$ (where γ is the Lorentz factor of the electrons, ranging from γ_{min} to γ_{max}), and a randomly oriented magnetic field B filling the dissipation region. The observer line of sight and the jet direction form an angle Θ_{view} . We parametrize the external radiation fields as proposed by Ghisellini & Tavecchio

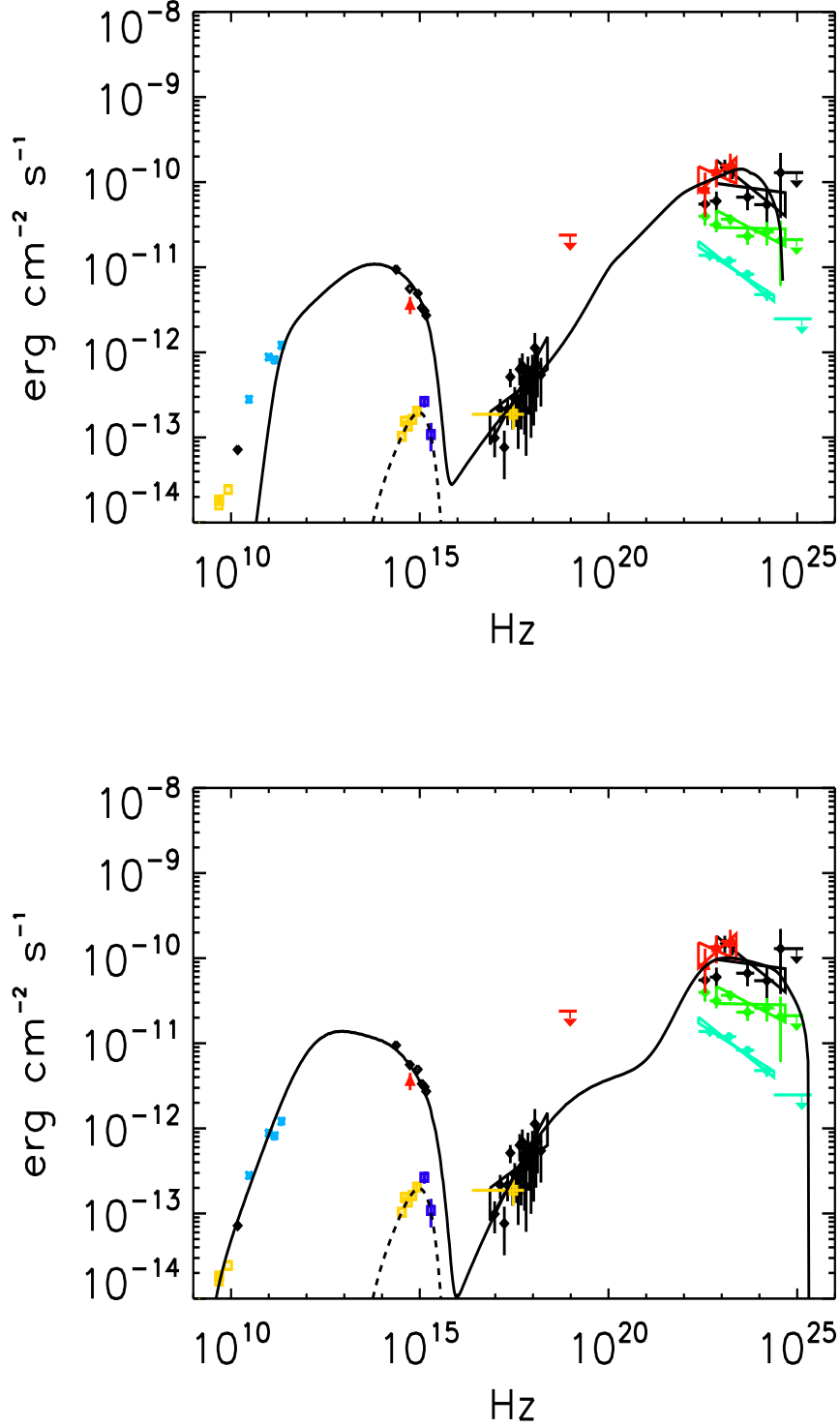


Figure 6. In the two plots we report the SEDs for the two high gamma-ray activity periods detected with *AGILE* (red symbols, data from *INTEGRAL*/OMC, *INTEGRAL*/IBIS, *AGILE*-GRID) and *Fermi*-LAT (black symbols, data from VLBA, Kanata, *Swift*/UVOT, *Swift*/XRT, *Fermi*-LAT) respectively. Green symbols are for data from *Fermi*-LAT integrated for one month period centered on the gamma-ray flare; light-cyan symbols are from the second *Fermi*-LAT catalog. We report optical data from SDSS (yellow) and UV data from GALEX (blue), as well as the Planck data (cyan), and the *ROSAT* detection (yellow) during the all-sky survey. Archival radio data from NED are shown in yellow. The disk model for the low activity period is plotted as a black dashed line; the model for jet emission in high activity period is reported as a continuous black line. In the top (bottom) plot we show the model assuming a blob dissipating at 0.2 pc (7 pc) from the central BH.

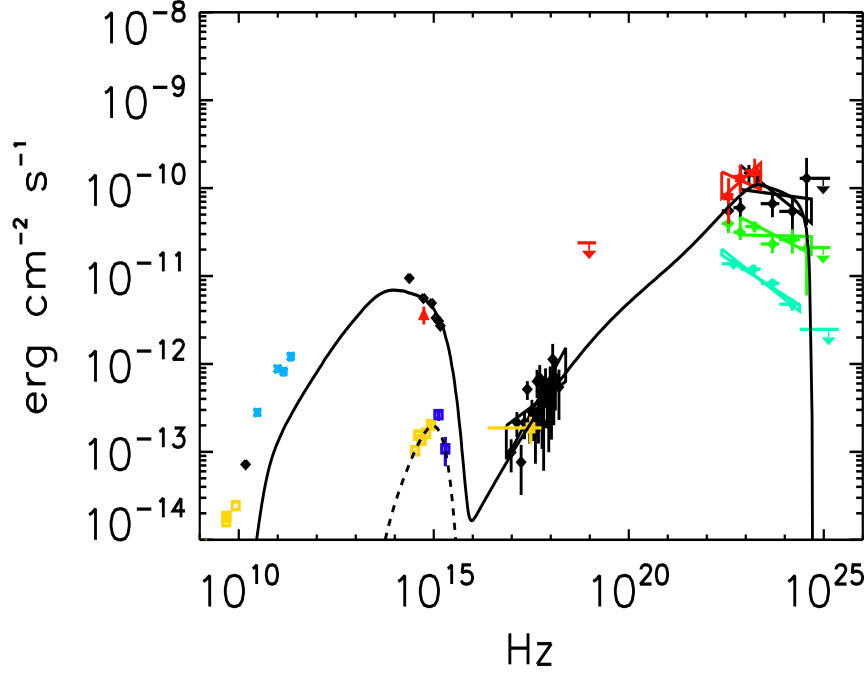


Figure 7. Same as previous figure, but in the jet emission model we assume a blob dissipating at ~ 5 pc, relaxing the condition $R_{blob} = \frac{1}{10} R_{diss}$, and assuming a blob radius of $\sim 10^{17}$ cm.

(2009), where the key elements are the accretion disk luminosity and the distance (R_{diss}) of the emitting blob from the central BH. We consider a jet aperture $\frac{R_{blob}}{R_{diss}} = 0.1$, according to Ghisellini & Tavecchio (2009). In evaluating the power carried by protons, we assume one proton per emitting electron. We assumed that during the campaigns A and B, the accretion disk luminosity is the same as the one obtained from the SDSS data in 2001 (dashed curve in Fig. 6). We found in section 5.4 that the *Fermi*–LAT gamma-ray spectrum (Fig. 6 green data, one month integration) does not show absorption from the BLR. Therefore, we tried to find solutions for the blob dissipating beyond the BLR, without taking into account the gamma-gamma absorption from the BLR. We obtained two possible solutions for the modeling. Model parameters are reported in Table 4, where we use R_{BLR} (R_{Torus}) to refer to the distance of the BLR region (of the dusty torus) from the BH; f_{BLR} (f_{Torus}) to the fraction of the disk emission that is reprocessed by the BLR in lines (by the dusty torus); ϵ_{accr} to the accretion efficiency; $\gamma_{cooling}$ to the electron Lorentz factor for which the electron energy halves in the blob crossing time (R_{blob}/c).

The first solution (model 1, top panel of Figure 6) places the dissipation region (R_{diss}) just beyond the BLR ($R_{diss} \sim 0.2$ pc from the SMBH), where the photon field from the dusty

torus is almost equal to the BLR seed photon field. At such a distance, the variability time-scale of a blob of radius $R_{blob} \sim 7 \times 10^{16}$ cm is of the order ~ 3 days, qualitatively in agreement (within a factor 2) with the 1-day binned gamma-ray light curve of the source. According to this modeling of the seed photon fields, the BLR photon contribution is expected to fade over time while the torus contribution remains constant. Both SSC and external Compton (EC) with seed photons from the torus contribute to the soft X-ray emission, the hard X-ray is dominated by EC emission with seed photons from the torus, and the GeV emission is dominated by EC with seed photons from the BLR. In the MeV up to GeV range the two EC contributions are almost equal. Further investigation of the variability is not possible, as no optical light-curve is available from which to trace the electron population from the synchrotron emission. Moreover the evolution of the gamma-ray photon index with time (reported in Fig. 4) is statistically poor.

The second solution to the SED modeling (model 2) has been found by assuming $R_{diss} \sim 7$ pc from the SMBH. Such a model requires a $R_{blob} = 2 \times 10^{18}$ cm, with a variability time-scale of the order of $\sim 10^2$ days. We do not find such a variability time-scale in the gamma-ray light curve, but we observe that the activity period for the source lasts at least 11 weeks. We can argue that the dissipating region in the jet has a radius of 2×10^{18} cm. Gradients of the electron energy density in the distance from the black hole, or disturbances in the jet (see for examples Giannios et al. 2010; Bromberg & Levinson 2009) can be responsible for the shorter variability observed in gamma-rays. With this model, the X-ray emission is due to SSC; the gamma-ray emission is due to EC with seed photons from the torus. The direct contribution of accretion disk photons to the EC is negligible.

In the model for a blob dissipating just beyond the BLR, the energy region below $\sim 10^{11}$ Hz is self absorbed. On the contrary, in the model of a distant dissipation region, there is no self-absorption, thus allowing the direct observation of radio emission from the blob. In this case, the emission predicted by the model is slightly higher than the flux reported in Fig. 6 (bottom panel), but we note that no radio observations were performed during the gamma-ray flares. The mismatch in the variability time-scale for model 2 with $R_{diss} \sim 7$ pc, results from the assumption that $R_{blob} = \frac{1}{10} R_{diss}$. Alternatively, we tried to model the SED assuming a blob of radius $\sim 10^{17}$ cm to satisfy the observed variability time-scale, and dissipating at ~ 5 pc from the SMBH (model 3). Model parameters are reported in the right column of Table 4, and the model is plotted in Fig. 7.

A similar kind of solution has been suggested by Tavecchio et al. (2011) to explain faster

Table 4. Model parameters for the fits of the spectral energy density, in the two assumptions of a blob dissipating just beyond the BLR ($R_{diss} \sim 0.2$ pc) or far away from the SMBH ($R_{diss} \sim 7$ pc). In the last column we report the model parameters for a blob dissipating far away from the SMBH ($R_{diss} \sim 5$ pc), but relaxing the condition $R_{blob} = \frac{1}{10} R_{diss}$, and assuming a blob radius of $\sim 10^{17}$ cm.

	model 1	model 2	model 3
$R_{diss}(pc)$	0.22	6.8	4.8
Blob radius (cm)	6.7×10^{16} *	2.1×10^{18} *	1×10^{17}
$m_{BH} (m_{\odot})$		5.3×10^8	
L_d (erg/s)		8.8×10^{45}	
R_{BLR} (cm)		3.0×10^{17}	
$R_{Torus}(cm)$		7.4×10^{18}	
f_{BLR}		0.1	
f_{torus}		0.3	
ϵ_{accr}		0.1	
Γ_{bulk}	20	20	20
angle of view (deg)	2	2	2
γ_{min}	1	1	1
γ_{max}	3.9×10^3	3.4×10^4	1.3×10^4
γ_{break}	0.95×10^3	1×10^3	1×10^3
density at γ_{break} (cm^{-3})	3.0×10^{-2}	1.5×10^{-4}	9.6×10^{-3}
s_1	1.1	0.5	1.3
s_2	3.1	3.3	2.5
B (Gauss)	6.1×10^{-1}	1.1×10^{-2}	7.6×10^{-2}
$\gamma_{cooling}$	60	1.1×10^4	2.4×10^3
electron power (erg/s)	2.2×10^{45}	4.5×10^{46}	1.1×10^{46}
magnetic power (erg/s)	2.5×10^{45}	7.9×10^{44}	8.6×10^{43}
proton power ** (erg/s)	1.1×10^{47}	1.6×10^{47}	3.0×10^{47}
radiated power (erg/s)	3.1×10^{45}	2.5×10^{45}	2.1×10^{45}

* $R_{blob} = \frac{1}{10} R_{diss}$ in this model.

** We assume one proton per emitting electron.

variability (of the order of 10 min) for PKS 1222+216. This model can correspond to a reconnection event, causing the acceleration of a small portion of the jet (Giannios et al. 2010), or to recollimation by the interaction with the external medium (Bromberg & Levinson 2009).

According to this SED modeling, the X-ray emission is due to SSC, and the gamma-ray emission to EC with external photons from the torus.

6 DISCUSSION AND CONCLUSIONS

We rarely have the opportunity to detect the disk emission in FSRQs, which are generally overwhelmed by synchrotron jet emission (see Pian et al. 1999, for example). However, our study here suggests that we have detected accretion-disk-dominated emission in GB6 J1239+0443. Granted, we cannot fully exclude the possibility that the archival SDSS and GALEX observations we have reported could be interpreted as other emission mechanisms than thermal disk emission because we lack strictly simultaneous radio observations and extended radio light curves to corroborate the assumption of low jet emission. However the assumption of disk emission remains, in our opinion, the most likely explanation for the observations.

The optical observations of GB6 J1239+0443 revealed an optical flux enhancement of a factor 15–30 in 6 years, signifying a shift from accretion-disk to synchrotron, jet-dominated emission. The optical spectrum obtained in the period of faint optical emission allowed the classification of the source as a FSRQ in BZCAT. We made an estimate of the SMBH mass of GB6 J1239+0443 and the accretion rate from a period of low jet activity. With these estimates, we were able to study the December 2008 flare. Modeling the observed flat gamma-ray spectrum and SED also allowed for an investigation into the location of the blazar-zone of the object.

As a final remark, it is worth stressing two major points. First, by definition, our estimate of R_{diss} is model dependent. The location of the dissipation region was estimated assuming the parametrization proposed by Ghisellini & Tavecchio (2009) for the BLR and the torus contribution to seed photons for the EC. According to this parametrization, it was possible to derive R_{diss} from the luminosity ratio of synchrotron to EC emission. In fact, in the parametrization by Ghisellini & Tavecchio (2009) for a dissipation region outside the BLR, the seed photons for EC fade with distance from the SMBH. We obtained two solutions. Referring to Figure 2 of Ghisellini & Tavecchio (2009), the ratio $\frac{U'_B}{(U'_{BLR}+U'_{IR})}$ equals the ratio of the optical to gamma-rays luminosity at the two values of the R_{diss} (assuming knowledge of the magnetic energy density). For the flares of GB6 J1239+0443 reported in this article, one solution (model 2) places the blob at $R_{diss} \sim 7$ pc, with only the dusty torus as the origin of seed photons. The other solution (model 1, with $R_{diss} \sim 0.2$ pc) corresponds to just outside the BLR, where the contribution of seed photons from both the dusty torus and the BLR are relevant. The magnetic field is constrained in the SED modeling by the cutoff of synchrotron

emission in the UV (due to the last and most energetic electrons), and by the corresponding cutoff of EC which we cannot derive directly from data (that give non-constraining upper limits at $E > 20$ GeV, see Fig. 6). Assuming the Thomson regime, and with only one external photon field contributing to the EC, the ratio f_{cutoff} between the synchrotron cutoff energy and the EC cutoff energy is proportional to $\frac{B}{\Gamma_{bulk} \langle \nu_{seed} \rangle}$, where $\langle \nu_{seed} \rangle$ is the typical seed photon field energy. Hence if we have constraining data at the highest energy, and with a specific geometry in the model, we can constrain B/Γ_{bulk} . However, the geometry in the model also constrains $U'_{BLR} + U'_{IR}$, hence in the ideal case we can obtain B/Γ_{bulk} and R_{diss} from the SED modeling. The ratio of synchrotron to SSC luminosity further constrains the model parameters R_{blob} , Γ_{bulk} , B , allowing one to remove the degeneracy between Γ_{bulk} and B . In reality, we can obtain only upper limits of f_{cutoff} because the data at higher energies are non-constraining. So we have only upper limits on B/Γ_{bulk} for each model. As a consequence, the $U'_{BLR} + U'_{IR}$ could be lower than in our parametrization (we have to maintain the ratio $\frac{U'_B}{U'_{BLR} + U'_{IR}}$ at the desired value). This implies that R_{diss} could be higher than our evaluations.

The second point is that the photon field intensity is proportional to the accretion disk luminosity, and the BLR and torus location is proportional to $\sqrt{L_d}$. In all our estimations, we assume that the disk luminosity is almost steady over time, e.g., in the low state observed during the Sloan Survey in 2002, during the GALEX observation in 2007, and during the gamma-ray flares observed by *AGILE* at the beginning of 2008 and by *Fermi*-LAT at the end of 2008. This assumption could be false. In this case, we observe that the parametrization of U'_{BLR} and U'_{IR} reported in equation (20) by Ghisellini & Tavecchio (2009) remains unchanged while varying L_d , provided that we scale the solution for R_{diss} with $\sqrt{L_d}$. Therefore, variations of the disk luminosity in time, and/or systematic errors in the evaluation of disk luminosity from our SDSS+GALEX data (possibly biased by jet emission) only slightly affect our estimation of R_{diss} .

The starting point of our modeling is that the emission region is far from the SMBH (at parsec scale), and we motivate this choice with the flat gamma-ray spectrum up to energies of 15 GeV. For a different approach and results for other blazars, we refer readers to the work of Tavecchio et al. (2010). They performed a detailed study of the localization of the emission region for bright blazars making use of the variability timescale for objects showing a spectral cut-off at $(10-20)/(1+z)$ GeV. They obtained that the variability timescale and spectra are in agreement with a dissipation region inside the BLR.

We note that, contrary to the model we used, some authors (e.g., Giommi et al. 2011, for example) model the SEDs of both FSRQ and BL Lacs with pure Synchrotron + Synchrotron Self Compton components only.

Model 1 ($R_{diss} \sim 0.2$ pc), gives a variability time scale of the order of 3 days, in agreement with the flare duration estimated from the 1-day binned gamma-ray light curve. This model, however, does not properly reproduce the flat gamma-ray spectrum. In particular, in order to reproduce the observed flux at energies > 10 GeV, it overestimates the spectrum for lower energies. On the contrary, model 2 ($R_{diss} \sim 7$ pc) reproduces the flat-gamma-ray spectrum, but it is not clear whether the predicted variability of the order of ~ 100 days can be associated with the duration of the gamma-ray activity period estimated from the 1-week/1-month binned gamma-ray light curves. The third model has been built by relaxing the relation $R_{blob} = 0.1 R_{diss}$ in order to preserve the variability time-scale estimated from the 1-day gamma-ray light curve (we follow the solution proposed by Tavecchio et al. 2011 for PKS 1222+216), and it still reproduces the gamma-ray spectrum. Interestingly, the size of the emitting region for PKS 1222+216 ($R_{blob} \sim 5 \cdot 10^{14}$ cm) and for GB6 J1239+0443 differ significantly.

For the third model, we obtain $R_{blob} = 0.0067 R_{diss}$, in agreement within a factor of two with the prediction of Bromberg & Levinson (2009), that gives $R_{blob} = 10^{-2.5} R_{diss}$, for the case of efficient conversion of bulk luminosity in radiation in the strong focusing scenario. With the same assumptions, Bromberg & Levinson (2009) assume that the location of the emitting region is at $R_{diss} \sim 2.5 (L_{jet}/10^{46} \text{ erg s}^{-1})(R_{BLR}/0.1 \text{ pc})^{-1}$ pc from the SMBH, where L_{jet} is the jet power. If we invert this relation, and we make use of our result ($R_{diss} = 4.8$ pc), we obtain $L_{jet} \sim 3.5 \cdot 10^{46} \text{ erg s}^{-1}$. We must assume that the proton-to-emitting electron ratio is of the order of 0.1 in order to reproduce such a power (in the evaluation of proton power reported in Table 4 we assumed one proton per emitting electron, instead). We note, however, that Nalewajko & Sikora (2009) evaluated that efficient radiative conversion could be assumed if the product of the bulk Lorentz factor by the opening angle is $\gtrsim 3$, and according to our third model this product is 2.

ACKNOWLEDGEMENTS

The authors wish to acknowledge the anonymous referee for his suggestions. We are also very grateful to J. Finke for comments and corrections, and for his careful proofreading of

several sections of this manuscript.

We acknowledge financial contribution from the agreement ASI-INAF I/009/10/0.

The *AGILE* Mission is funded by the Italian Space Agency (through contract ASI I/089/06/2) with scientific and programmatic participation by the Italian Institute of Astrophysics (INAF) and the Italian Institute of Nuclear Physics (INFN).

This research has made use of data from the MOJAVE database that is maintained by the MOJAVE team (Lister et al. 2009).

This research has made use of the NASA/IPAC Extragalactic Database (NED) which is operated by the Jet Propulsion Laboratory, California Institute of Technology, under contract with the National Aeronautics and Space Administration.

This research has made use of the SIMBAD database, operated at CDS, Strasbourg, France. RJA is supported by an appointment to the NASA Postdoctoral Program at the Jet Propulsion Laboratory, administered by Oak Ridge Associated Universities through a contract with NASA.

The *Fermi* LAT Collaboration acknowledges generous ongoing support from a number of agencies and institutes that have supported both the development and the operation of the LAT as well as scientific data analysis. These include the National Aeronautics and Space Administration and the Department of Energy in the United States, the Commissariat à l’Energie Atomique and the Centre National de la Recherche Scientifique / Institut National de Physique Nucléaire et de Physique des Particules in France, the Agenzia Spaziale Italiana and the Istituto Nazionale di Fisica Nucleare in Italy, the Ministry of Education, Culture, Sports, Science and Technology (MEXT), High Energy Accelerator Research Organization (KEK) and Japan Aerospace Exploration Agency (JAXA) in Japan, and the K. A. Wallenberg Foundation, the Swedish Research Council and the Swedish National Space Board in Sweden. Additional support for science analysis during the operations phase is gratefully acknowledged from the Istituto Nazionale di Astrofisica in Italy and the Centre National d’Études Spatiales in France.

REFERENCES

- Abdo A. et al., 2010, *ApJL*, 714, L73-L78;
 Adelman McCharty J. K., et al., 2008, *ApJS*, 175, 297;

- Agudo I. et al., 2011, ApJL, 726, 13;
Agudo I. et al., 2011, ApJL, 735, 10;
Assef R. J., et al., ApJ in press; arXiv:1009.1145;
Atwood et al., 2009, ApJ, 697, 1071-1102;
Bottcher M., Ap&SS, 2007, 309, 95-104;
Bromberg O.& Levinson A., 2009, ApJ, 699, 1274-1280;
Burrows D. N., et al. 2005, Space Sci. Rev., 120, 165;
J. M. Casandjian, I. A. Grenier, 2008, A&A, 489, 849;
Cattaneo P. W. et al., 2011, NIMA, 630, 251-257;
Collin S. et al., 2006, A&A, 456, 75;
Dickey J. M. & Lockman F. J. , 1990, ARA&A 28, 215-261;
Denney K. D., et al., 2009, ApJ 692, 246;
Denney K. D., et al., 2011, PoS (NLSY1), 34;
Esposito J. A. et al., 1999, ApJS, 123, 203-271;
Finke J., et al., 2010, ApJ, 712, 238-249;
Fitzpatrick E. L., 1999, PASP 111, 63-75;
Gehrels N., et al. 2004, ApJ, 611, 1005;
Ghisellini G. et al. 2007, MNRAS, 382, L82-L86;
Ghisellini G. & Tavecchio F., 2009, MNRAS, 397, 985-1002;
Ghisellini G. et al., 2010, MNRAS, 402, 497;
Ghisellini G. et al., 2011, MNRAS, 411, 911;
Giannios D. et al., 2010, MNRAS, 402, 1649-1656;
Giommi P. et al., 2011, A&A submitted; arXiv:1108.1114v1;
Hartman R. C., et al., 1999, ApJS, 123, 79-202;
Ikejiri Y., 2009, Atel 1892;
Ivezic., et al., 2007, ASPC, 364, 165-175;
Jester S., 2005, AJ 130, 873;
Jorstad S. G. et al., 2010, ApJ, 715, 362-384;
Lister M. L., et al., 2009, AJ, 137, 3718;
Maraschi L., Ghisellini G., and Celotti A., 1992, ApJL, 397, L5-L9;
Marscher A. P., and Bloom S. D., 1992, Proceedings of The Compton Observatory Science Workshop, 346-353;
Marscher A. P., et al., 2010, ApJL, 710, 726;

- Martin D. C. et al., 2005, *ApJL*, 619, L1-L6;
- Mas-Hesse J. M., et al. 2003, *A&A*, 411, L261;
- Massaro E., et al., 2010; arXiv:1006.0922;
- Mattox J. R., Bertsch, D. L., Chiang, J., et al., 1996, *ApJ*, 461, 396-407;
- Mücke A., Protheroe R. J., 2001, *Astropart. Phys*, 15, 121-136;
- Mücke A. et al, 2003, *Astropart. Phys*, 18, 593-613;
- Nalewajko K. & Sikora M., 2009, *MNRAS* 392, 1205;
- Nolan P. L. et al., 2012, *ApJS*, 199, 31;
- Pacciani L., et al., 2009, *A&A*, 494, 49;
- Pian E. et al., 1999, *ApJL*, 521, 112;
- Pittori C., et al., 2009, *A&A*, 506, 1563;
- Poole T. S., Breeveld A. A., Page M. J., et al., 2008, *MNRAS*, 383, 627
- Poutanen J & Stern B., 2010, *ApJL*, 717, 118;
- Richards G. T., et al., 2002, *AJ*, 124, 1;
- Roming P. W. A., et al. 2005, *Space Sci. Rev.*, 120, 95;
- Shakura N. I. & Sunyaev R. A., 1973, *A&A*, 24, 337;
- Shaw M. S., et al., 2012, *ApJ*, in press;
- Sikora M., Begelman M. C., and Rees M., 1994, *ApJ*, 421, 153;
- Sikora M., et al., 2008, *ApJ*, 675, 71-78;
- Tavani, M., Barbiellini, G., Argan, A., et al., 2009, *A&A*, 502, 995-1013
- Tavecchio F. & Mazin D., 2009, *MNRAS*, 392, L40-L44;
- Tavecchio F. et al., 2010, *MNRAS*, 405,L94-L98;
- Tavecchio F. et al., 2011, *A&A*, 534, A86;
- Terasranta H. et Al., 2005, *A&A*, 440, 409;
- Tramacere A., et al., 2009, *Atel.* 1888;
- Ubertini P., et al., 2003, *A&A*, 411, L131-L139;
- Urry C. M., and Padovani P., 1995, *PASP*, 107, 803;
- Verrecchia F. et al., 2011, *ASR* in press, doi:10.1016/j.asr.2011.05.035;
- Vestergaard M., Peterson B. M., 2006, *ApJ*, 641, 689;
- Watanabe M., et al. 2005, *PASP*, 117, 870-884;
- Winkler C, et al. 2003, *A&A*, 411, L1.